Global Research journal of Natural Science and Technology (Grjnst)
Volume: 03 - Issue 4 (2025)
p.ISSN: 2790-7643 e.ISSN: 2790-7651

Cross-Dataset Generalization of RCED-UNet3+ for Robust Lung Nodule Segmentation

Sadaf Raza
Assistant Professor, Department of Electronic Engineering, Sir Syed University of Engineering & Technology, Pakistan
Razia Zia
Associate Professor, Department of Computer Science, Faculty of Engineering Science and Technology, Iqra University, Pakistan
Irfan Ahmed Usmani
Assistant Professor Department of Biomedical Engineering, Salim Habib University (Formerly Barrett Hodgson University), Pakistan
Noman Ahmed Siddiqui
Assistant Professor, Department of Electronic Engineering, Sir Syed University of Engineering & Technology, Pakistan
Natasha Mukhtiar
Lecturer, Institute of Biomedical Engineering & Technology, Liaquat University of Medical & Health Sciences Jamshor, Pakistan
Corresponding Author Email: sminhaj@ssuet.edu.pk[1]
DOI:

ABSTRACT

Aim of the Study: The main objective of this study is to ensure that pulmonary nodules are properly identified on CT scans to detect lung cancer at the earliest stage. In particular, the study aims to assess the generalizability and robustness of the RCED-UNet3+ segmentation model across datasets with varying imaging properties.

Methodology: The current study is a continuation of our earlier work in which the RCED-UNet3 + model has a Dice score of 0.984 on the LIDC-IDRI dataset. The model will be further evaluated on the LUNA16 dataset to extend the results achieved previously. The datasets also vary in terms of scanner technologies and image resolutions, and hence offer a platform to evaluate the model in terms of its consistency in performance in different imaging sources. The p-value analysis ($p < 0.05$) was used to test the statistical significance in order to confirm the model consistency.

Findings: RCED-UNet3+ model had high generalization potential with a Dice score of 0.980 with consistent Intersection over Union (IoU) value of 0.961 on the Luna16 dataset. The findings validate the observation that segmentation accuracy of the model is also consistent despite changes in imaging parameters.

Conclusion: The research establishes that RCED-UNet3+ is a stable and efficient segmentation model in the detection of lung nodules. Its capability of sustaining high performance in datasets that contain mixed imaging properties of heterogeneous nature suggests its high potential integration into clinical workflows that seek to result in early and precise lung cancer diagnosis.

Keywords: Deep Learning, Lung cancer, Segmentation, RCED-UNet3+, LIDC-IDRI, LUNA16

1.INTRODUCTION

The respiratory diseases remain among the leading causes of death in the world. Asthma, chronic obstructive pulmonary disease (COPD), acute respiratory infection, tuberculosis, and, in particular, lung cancer are conditions that represent a serious threat to public health (Soriano et al., 2020). Lung cancer is still one of the fatal types of cancer, and the 2025 calculation relates to the number of 2.2 million newly diagnosed cases and approximately 1.79 million deaths on a worldwide basis (Seidel et al., 2025). Most patients however, get their diagnosis at an advanced stage when treatment is minimal and the survival rate is reduced to about 3.9%. Conversely, early detection of the disease can increase survival rate to almost 54% in most cases by early screening (Frimino et al.,). Computer Tomography (CT) has been found to be very effective in identifying lung cancer at its early stages and as a result it can be used as an important tool in minimizing the number of deaths caused by the disease. Manual analysis of CT scans is very labour intensive and time consuming since different physicians may have different clinical interpretations.

To address this problem, computer-aided diagnosis (CAD) systems have been developed to assist radiologists (Zemouri et al., 2019). The initial and the most significant stage of automated thoracic imaging is usually lung segmentation (Mansoor et al., 2015) (Hofmanniger et al., 2020). The advantage of this step is the ability to remove irrelevant data by isolating the lung areas, enabling machine learning-based features to concentrate on diagnostically relevant aspects, making the processing faster and more predictable (Chatuevedi et al., 2021).
Segmentation of the lungs is highly difficult due to the fact that the lung structure, size and capacity differ among patients. The existence of other conditions like lung consolidation or cavities in lung tissue also complicates such problems and could be a limitation to the effectiveness of segmentation methods (Mansoor et al., 2015). Most of the computation methods demonstrate excellent performance with normal shapes but fail in challenging clinical scenarios. The primary reason why this problem occurs is the small range of training data employed to develop these models (Hofmanniger et al., 2020). Before the development of deep learning, several conventional machine learning approaches were proposed to the lung nodule segmentation problem. These were rule-based methods, intensity algorithms, morphological processes, level-set model, graph-cut methods, thresholding, and region-grow methods (Diciotti et al., 2008) (Boykov et al., 2004). A framework to segment nodules on a rolling ball filter using a rule-based framework was proposed in (Messay et al., 2010). Yuan et al. (Yuan et al., 2012) proposed level sets and graph cuts energy minimization methods whereas Demeshki et al. (Demeshki et al., 2008) proposed a contrast-based region-growing algorithm. Kostis et al. (Kostis et al., 2003) used morphological opening procedures, in addition to connected component analysis, to outline the lung nodules and isolate them against vascular structures in the surrounding. Techniques based on region growing typically needed a manually selected seed point in order to begin segmentation. To extract shape and texture features, Filho et al. (Filho et al., 2014) first used Gaussian and median filtering of the lung parenchyma and then used a threshold method to segment and extract the features. False positives were then removed using a Support Vector Machine (SVM). Jacobs et al. (Jacobs et al., 2014) created a twenty-one contextual feature, which is based on the grayscale intensity, shape, and texture descriptors, and significantly enhanced the classification rates. Nevertheless, these traditional approaches are mostly depend on manual feature engineering in order to perfectly segment the area of interest. Moreover, they tend to have a problem in differentiating nodules which are

attached to the pleural wall. Because the extracted features are manually derived using the raw image data, the information is invariably compressed during the process, hence decreasing the representation of the original input.

Over the past decade, deep neural networks have become the leading methods in medical imaging analysis. They show better performance than traditional image processing techniques. The U-Net architecture, and its variants, excelled in the field of medical image segmentation. Skourt et al. (Skourt et al., 2018) created a segmentation technique that is grounded on the U-Net design. They developed four consecutive module encoding pathway. There were two convolutional operations with ReLU functions of activation and maximum pooling processes in each of the modules. The decoding pathway was also identical, but up-sampling technique and residual links were used to preserve the spatial resolution. Research that used the LIDC-IDRI database, whose reference annotations are rigorously checked, has shown that the technique is valid . Modified U-Net, as given by Shaziya et al. (Shaziya et al., 2018) included an encoding section with three convolutional modules, all of which had ReLU activation and then max-pooling functions in order to achieve precise pulmonary segmentation. Three decoding stages were incorporated in the decoding section. The initial two stages consisted of two convolutional stages with residual links and the last stage contained three convolutional stages with additional convolutional stages and a dropout network, and the final segmentation output layer. Original images of 128x128 pixels were downsampled to 32x32 to enhance the computing speed. Moreover, Yoo et al. (Yoo et al., 2020) created two variations of U-Net models, one is a two-dimensional U-Net and the other a three-dimensional one, to use in pulmonary segmentation tasks. They used structures of the lungs as single organs or as right and left parts of the anatomy. The two-dimensional network they used was 512x512x1 pixel, which involved four stages of decoding and encoding, where they used bilinear interpolation in the up-sampling stages. In contrast, the 3D model accepted 512×512×8 input volumes and featured three down sampling and three up sampling blocks, with trilinear interpolation used in the latter. A softmax function was employed at the output, with cross-entropy as the loss function. In this study, two distinct models were developed one designed to segment both lungs together, and another focused on segmenting the left and right lungs separately. To facilitate this, the original ground truth annotations were divided into two binary masks, each corresponding to one lung. These masks were then horizontally flipped to augment the dataset, effectively generating additional training samples for the opposite lung.

Segmenting the lungs from CT images remains a highly complex task, especially due to overlapping imaging features from coexisting diseases. Other respiratory diseases are also common in lung cancer patients. As an illustration, lung cancer and chronic obstructive pulmonary disease (COPD), which are commonly associated with tobacco consumption, are both visually similar but differ in their imaging appearances. Thus, in addition to detecting abnormalities associated with lung cancer, segmentation algorithms should be in a position to detect features that are the indicators of other lung diseases. In segmentation of lung nodules, the recent advances have focused on enhancing the accuracy and reliability of deep learning methods. An example of such a development is the RCED-UNet3+ model, which modifies the normal UNet3+ model by introducing residual connections into both encoder and decoder layers (Raza et al., 2024). This can be used to preserve gradient flow, which is effective in overcoming many problems such as vanishing gradients and in improving the capability of the model to learn fine features particularly in cases where small nodules or irregular shaped nodules are involved. In the LIDC-IDRI dataset, the model performed well, reaching the Dice score of 0.984 and IoU at 0.979 with the help of data augmentation. The model works perfectly well on this dataset, but its generalization to other datasets, including LUNA16, still needs to

be investigated. Thus, the proposed study is aimed at assessing generalization performance of the RCED-UNet3+ network in the application to the LUNA16 dataset as an external test set.

2. METHODOLOGY

The following section introduces the RCED-UNet3+ model, which was trained on the LIDC-IDRI dataset and tested on the LUNA16 and LIDC-IDRI datasets, demonstrated in Figure 1 (Raza et al., 2024). RCED-UNet3+ model is the enhancement of the baseline UNet3+ model that incorporates the residual connection both in the encoder and decoder that enhances feature extraction and solves the network degradation during training. Testing is conducted with the help of various data sets. The hybrid loss is used to enhance the quality of segmentation. The implementation process is given in the following section.

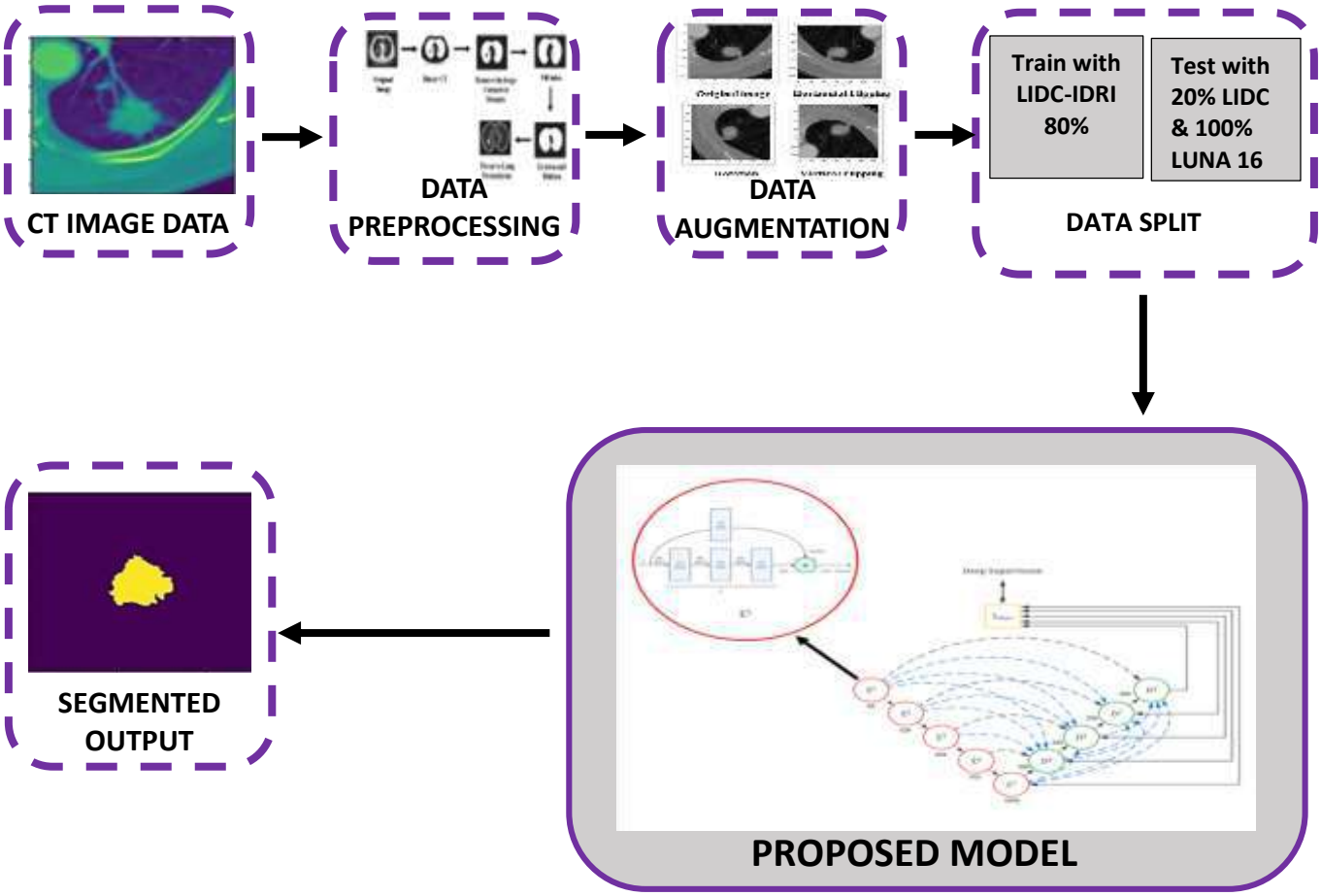

Figure 1. *The proposed RCED-UNet3+ segmentation framework is trained using the LIDC-IDRI dataset and evaluated on the LUNA16 dataset to assess its cross-dataset generalization*

2.1 Dataset

To train a model, 1,018 CT scans of 1,010 patients were obtained from the LIDC-IDRI dataset, each scan was annotated by a professional radiologist. This dataset consists of 15,550 image slices highlighted with the lung nodules. In order to determine how well the model can be generalized to other datasets, the LUNA16 dataset was used to test the model. It is composed

of 1,186 annotated nodules derived out of 888 cases. The two datasets are both in DICOM format and they have structural consistency. In contrast to some datasets, like DSB, which contain the only patient-level labels, LUNA16 gives the region-level annotations.

2.2 Preprocessing

Preprocessing of CT scan is aimed at separating the lung parenchyma against other structures like bed frames, muscles and bones to limit external interference. Since nodules are limited to the parenchymal region in the lungs, accurate segmentation of the region is essential in reducing false positives as well as improving segmentation accuracy using CT images. Low-intensity grayscale areas are seen in the lung parenchyma, and higher grayscale values are seen in the surrounding chest muscles in CT. Lung parenchyma segmentation is a complicated multi-step process. The initial step is generally binarization, in which CT images are converted into binary, that is, lung tissues are represented by black and the other structures by white using thresholding. Morphological dilation is then used to fill small gaps left behind by more dense tissues. This operation dilates the lung boundaries by filling small discontinuities or holes in the area. The result is a detailed representation of the lung parenchyma. The step-by-step process of segmentation of the lung parenchyma on CT images is shown in Figure 2 (Raza et al., 2024).

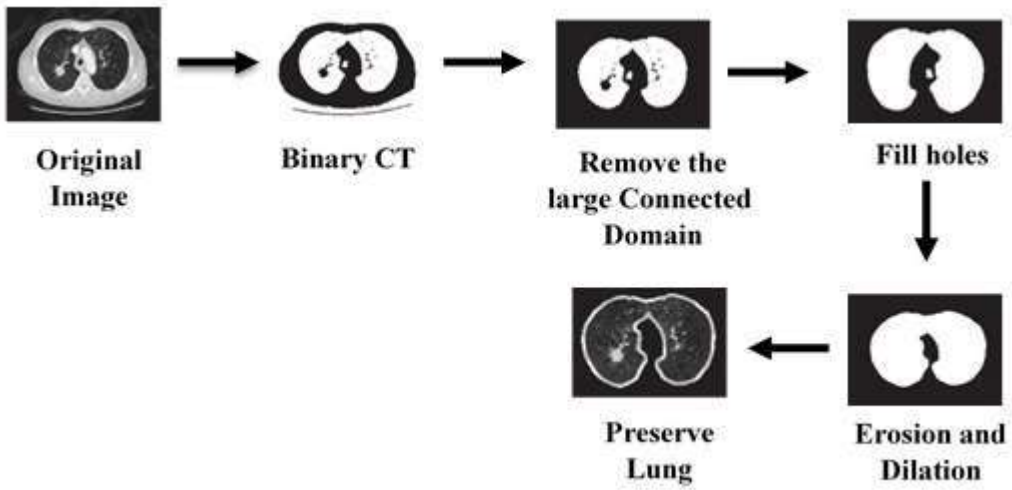

Figure 2: *Step-by-step procedure for extracting lung parenchyma regions from CT image.*

2.3 Data Augmentation

Data augmentation was employed to enhance the ability of the model to learn new patterns and how it would perform in other conditions. This was done in three geometric transformations, i.e. horizontal flip, vertical flip and rotation. The initial CT image was transformed into three additional images and the total number of sample achieved was 62,200. Figure 3 presents an example of the three techniques used to obtain invariance to geometric transformations (Raza et al., 2024).

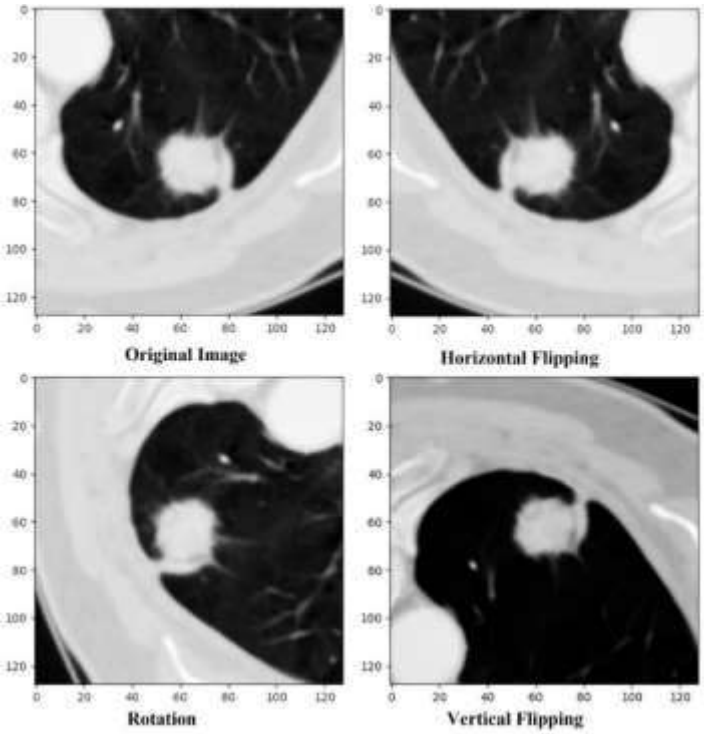

Figure 3: *The original image with three transformation-based variants applied for data augmentation.*

2.4 Methodology

The proposed study suggests an improved architecture called RCED-UNet3+ (Raza et al., 2024), which is based on the already existing UNet3+ architecture. It is particularly designed to explore how the model can be generalized to diverse medical image data sets. The proposed architecture adds residual connections in both direction paths, which are designed to preserve the features and overcome issues such as vanishing gradient and information loss that normally occur in the more complex convolutional networks. The proposed encoder structure of RCED-UNet3+ is shown in Figure 4 (Raza et al., 2024).

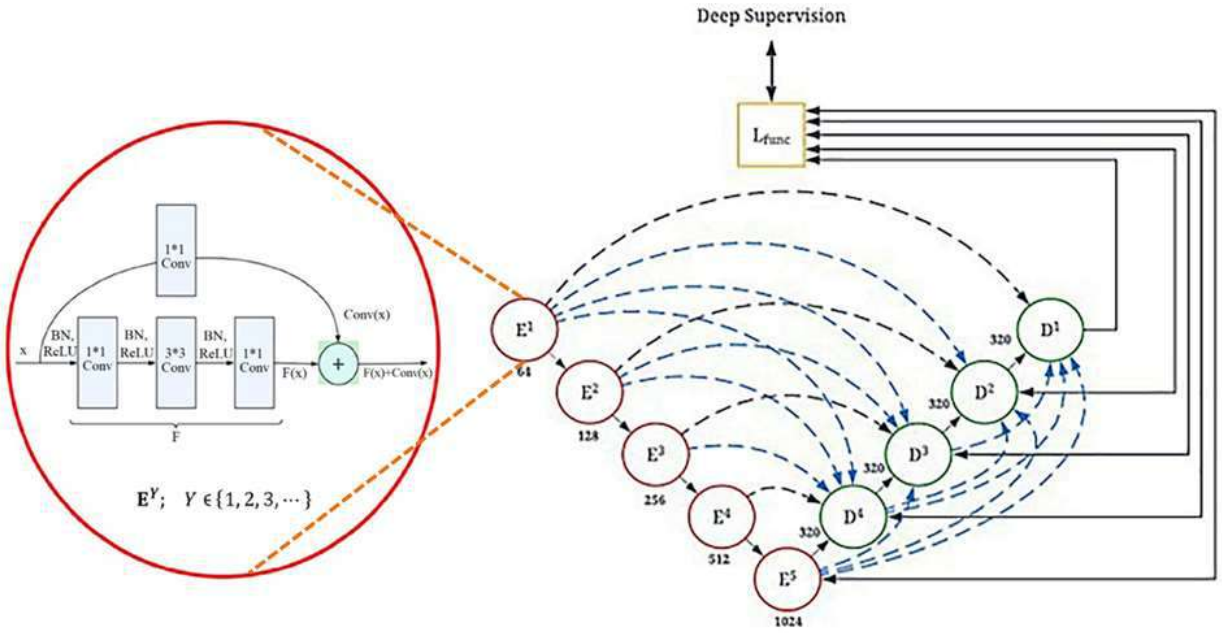

Figure 4: *Structural layout of the encoder module in the RCED-UNet3+ framework.*

2.4.1 *Advancing Beyond UNet++ and UNet3+ Limitations*

Earlier extensions of UNet, such as UNet++ and UNet3+, brought improvements through better skip connections and added multi-scale deep supervision. Nevertheless, the basic encoder-decoder system did not change significantly. This is an architectural drawback that limits their performance in the segmentation of lung nodules with complex edges or low contrast. To overcome this, the RCED-UNet3+ brings improvements that maintain the spatial and semantic integrity (Raza et al., 2024).

2.4.2 *Residual Block Integration for Stronger Feature Representation*

To enhance the learning and gradient flow, the architecture incorporates residual blocks into every level of the encoder and decoder. These blocks consist of three consecutive convolution operations with 1∗1, 3∗3, and 1∗1 kernels. Each layer is followed by:

- Batch Normalization to maintain stable activation distributions
- ReLU activation to introduce non-linearity for richer feature extraction

The residual output is calculated as defined in Equation 1.

$$RC = x + F(x) \quad (1)$$

If input and output dimensions differ, the input is passed through a 1∗1 convolution with padding to ensure compatibility, and the residual connection is defined in Equation 2.

$$RC = Conv(x) + F(x) \quad (2)$$

This residual mechanism supports more efficient training and helps maintain critical details, which is especially valuable in segmenting subtle or small lung nodules.

2.4.3 *Preserving Key Features with Deep Supervision and Multi-Scale Fusion*

The RCED-UNet3+ also retains the core innovations of UNet3+, namely:

- **Deep supervision**, allowing intermediate outputs to contribute directly to the final prediction
- **Multi-scale skip connections**, which fuse contextual details across different resolutions

These mechanisms collectively allow the model to localize features more precisely, especially in anatomically complex regions.

2.4.4 *Dataset Strategy for Generalization Testing*

To evaluate how the model will perform on unknown data, it is being trained using LIDC-IDRI data which contains detailed and extensive annotations. The model has been tested on the LUNA16 dataset a collection that is not similar regarding structure and data distribution. A cross-dataset evaluation method would provide a more accurate estimate of the generalization capability of the model across the different imaging sources.

2.4.5 *Accuracy and Effectiveness in Segmentation*

The performance evaluation of the RCED-UNet3+ model achieved a Dice Similarity Score of 0.980 that is significantly higher than the 0.942 of the baseline UNet3+ model. This great rise shows the benefit of utilizing residual connections that may enhance precision of segmentation and the flexibility of the model when data of different properties are utilized.

3. EXPERIMENTAL SETUP

The performance of the model was evaluated in two ways. The initial experiment tests the original UNet3+ model. The second experiment involved the RCED-UNet3+ that incorporates residual connections to enhance feature extraction and representation. Both of the models were trained using CT scans LIDC-IDRI dataset, and were tested on LIDC-IDRI and LUNA 16. This indicates that they can generalize the cases of different patients.

The LIDC-IDRI dataset which consists of 15,550 CT slices, individual CT slices were annotated by four experienced radiologists and this ensured that the boundaries of pulmonary nodules were reliably delineated. Preprocessing steps before training had been applied to separate the lung parenchyma and eliminate any irrelevant anatomy and imaging artifacts to enhance the quality of the input data. The augmentation methods of rotation, scaling, and flipping were used to reduce the possibility of overfitting and increase the variability of the dataset. These processes increased the number of images to 62,200, which eventually gave the models a wider range of diversity and more realistic training.

The Python language was used to develop the models based on the PyTorch framework. The choice of hyperparameters was based on the best practices in the reference study (Aversano et al. 2022), and only the formulation of the loss function was changed. The configuration parameters involved in training were a learning rate of 0.01, a dropout rate of 15 percent, a batch size of 32 samples, and Stochastic Gradient Descent to optimize the parameters.

The hybrid loss was a composition of dice loss and binary cross-entropy loss defined in Equation 5. Dice loss is used to measure the likelihood similarity of predicted segmentation masks to the ground truth annotations defined in Equation 3, whereas binary cross-entropy loss

is used to measure errors in the classification of individual pixels, defined in Equation 4. The dual-component approach allows the network to achieve high precision of segmentation and increase the accuracy of boundary definition.

Dice Loss:

$$l_{DLS} = 1 - \frac{2CS+1}{C+S+1} \quad (3)$$

Binary Cross-Entropy Loss:

$$l_{BCE=} Clog(s) + [(1 - Clog(1 - S)] \quad (4)$$

Combined Loss:

$$l_H = l_{DLS} + l_{BCE} \quad (5)$$

Dice Similarity Coefficient (DSC) defined in Equation 6, and Intersection over Union (IoU) is defined in Equation 7, were the two measures to determine the accuracy of the segmentation. By examining the locations of pixel values in the two segmentations, these two approaches verify the similarity between the ground truth masks and the predicted values of the model. Here, C denotes the ground truth mask, while S refers to the model's output.

Dice Coefficient:

$$Dice = 2 * |C \cap S| / (|C| + |S|) \quad (6)$$

IoU Score:

$$IoU = /C \cap S/ / /C \cup S/ \quad (7)$$

These evaluation measures are commonly used in medical image analysis, especially for segmentation tasks involving small and intricate anatomical features like lung nodules.

4. RESULTS AND DISCUSSION

The RCED-UNet3+ model was evaluated using segmentation metrics (Dice Similarity Coefficient (DSC) and Intersection over Union (IoU)). The results obtained by RCED-UNet3+ were better than the baseline UNet3+ on the LUNA16 dataset as indicated in Table 1. This enhancement of consistency means that the model possesses the generalization property and can be able to preserve its accuracy with new CT images, which is essential to its clinical application.

Table 1: *Comparative performance metrics of UNet3+ and RCED-UNet3+ models on LUNA16 test images.*

Model	Mean IoU Score	Mean Dice Score
UNet3+	0.901	0.942
RCED-UNet3+	0.961	0.980

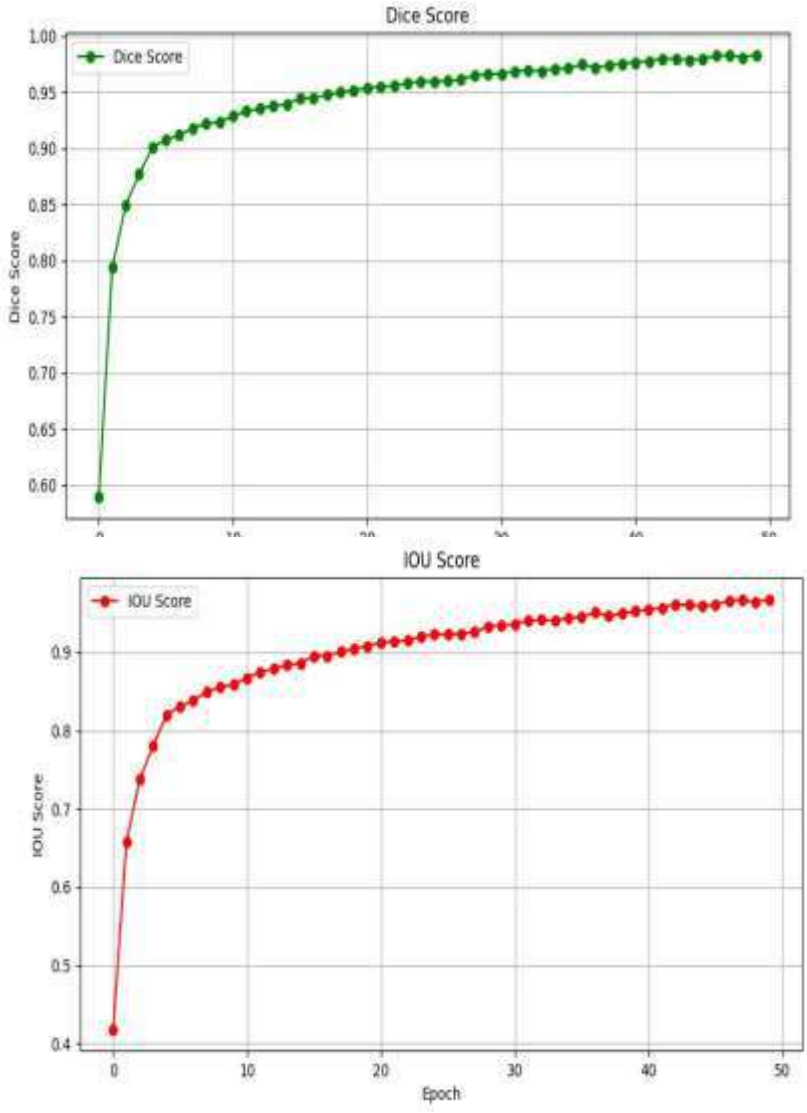

Figure 5: *Progression of Dice and IoU metrics over training epochs*

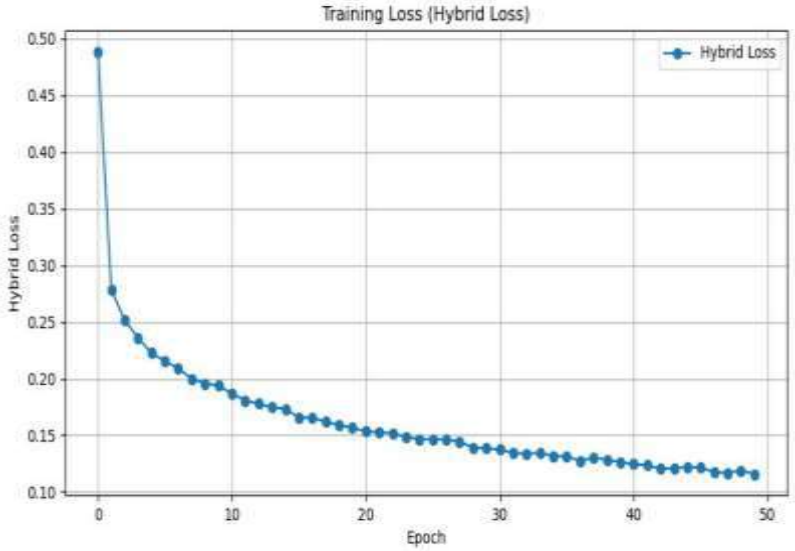

Figure 6: *Change in hybrid loss across epochs, reflecting model optimization on the training set.*

Figure 5 represents the trends of training by illustrating the evolution of Dice and IoU values throughout the training epochs. RCED-UNet3+ was always the best in comparison with the baseline model, and the improvements improved consistently with the further training. A hybrid loss (a combination of Dice loss and Binary Cross-Entropy) was used, which helped to achieve a stable and more consistent convergence. This is further demonstrated in Figure 6, where the loss steadily declines over the training period, reflecting the model's ability to learn complex nodule patterns more effectively.

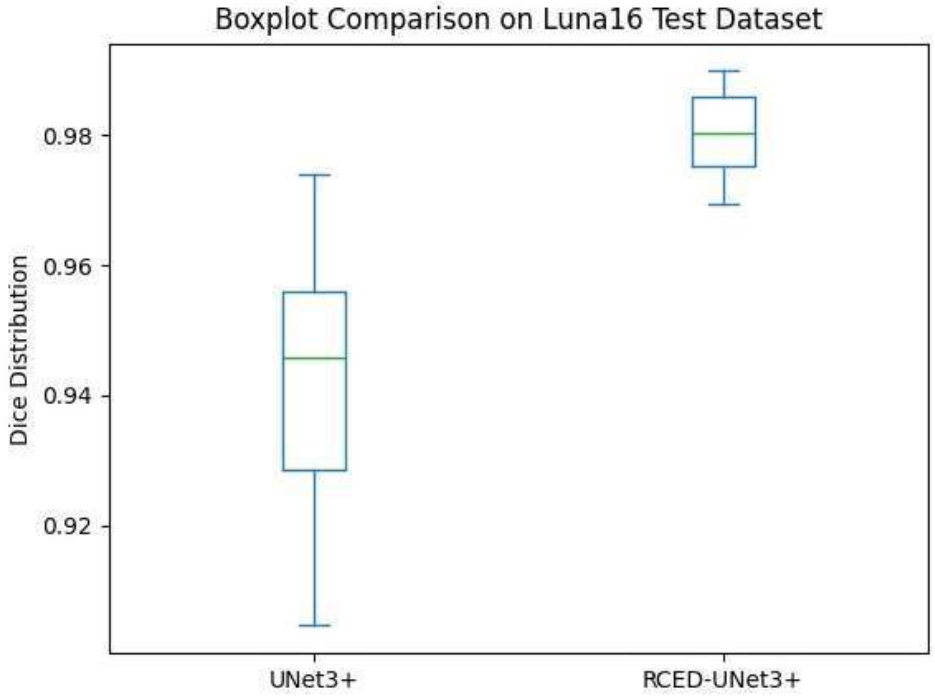

Figure 7: *Boxplot comparison of UNet3+, RCED-UNet3+ on LUNA16 Test data*

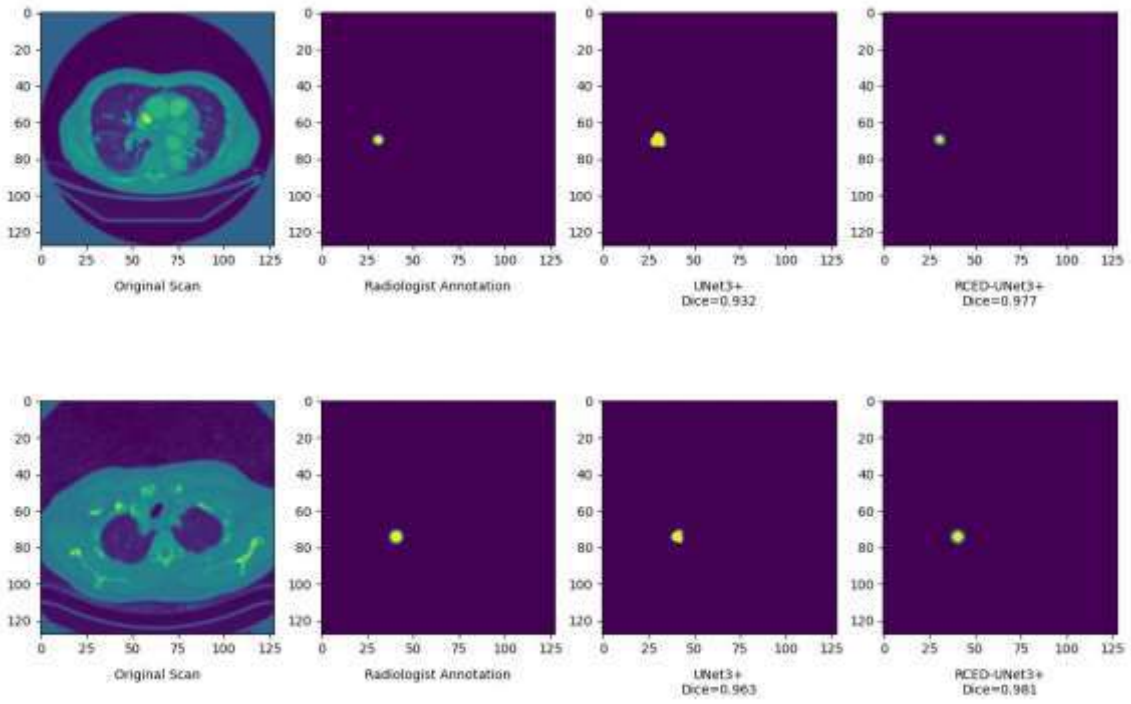

Figure 8: *Qualitative evaluation of UNet3+ and RCED-UNet3+ outputs compared with radiologist-marked ground truths on LUNA16 test images.*

Figure 7 presents a boxplot analysis that depicts the min and max score ranges and distribution of Dice score on the test samples and Figure 8 provides the qualitative assessment. The RCED-UNet3+ model with augmented data showed the best median results as well as the smallest interquartile range, which implies consistent and similar performance across cases.

In order to assess the strength of the generalization of the RCED-UNet3+ framework in a comprehensive manner, the assessment of the statistical evaluation was performed in addition to the traditional use of the Dice and IoU scores. Figure 9 illustrates a direct comparison of the means of the Dice scores achieved by UNet3+ and RCED-UNet3+ on LUNA16 dataset. It also has the 95 percent confidence interval bars, which themselves indicate the consistency of the performance of each model. The confidence intervals are not overlapping, and RCED-UNet3+ has a significantly higher mean score, which is a statistically acceptable evidence ($p < 0.05$) of greater accuracy of segmentation.

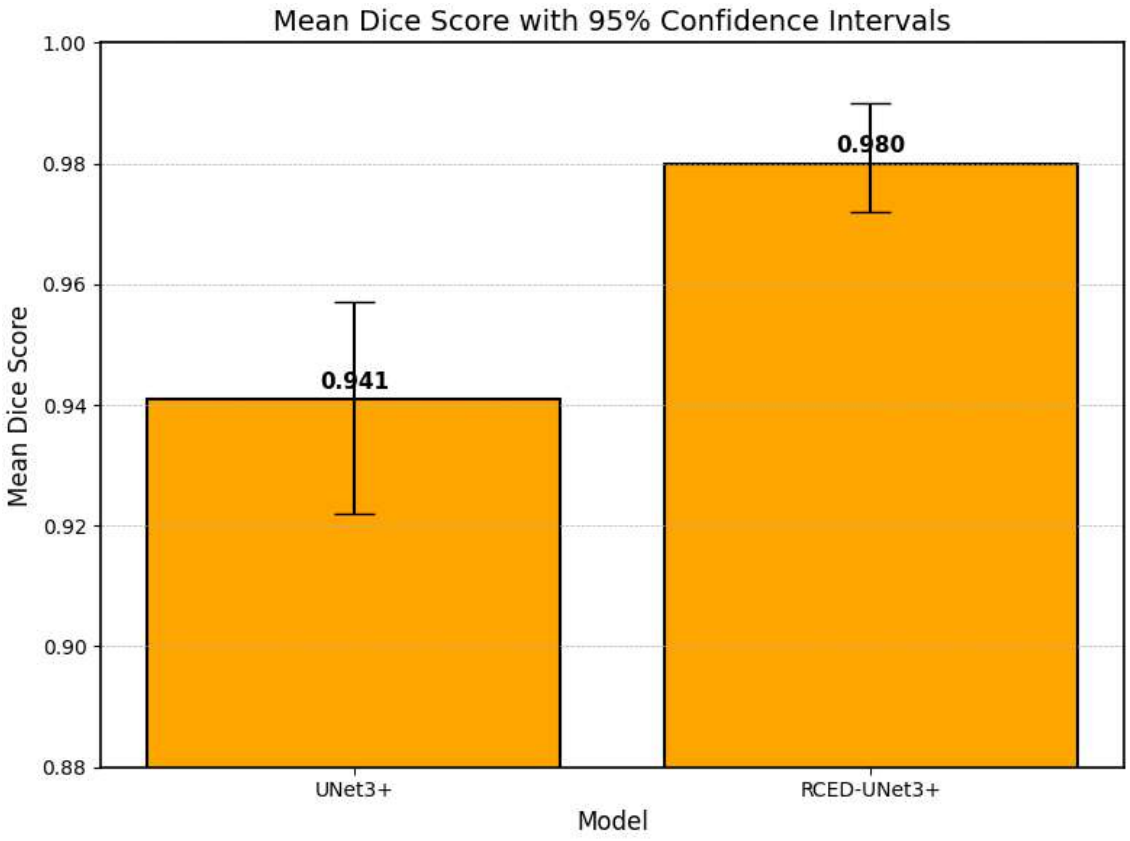

Figure 9: *Average Dice scores with 95% confidence limits show RCED-UNet3+ clearly outperforms UNet3+ on the LUNA16 dataset*

Furthermore, **Figure 10** illustrates a **Bland–Altman analysis**, used to evaluate the agreement between the two models on a per-sample basis. The vertical axis shows the Dice score difference for each case, while the horizontal axis represents the average of both models' predictions. Most of the points fall within the ±1.96 standard deviation ranges, which is an indication of consistent behavior with a diverse sample. The resulting mean difference of -0.039 shows that there is a noticeable bias towards RCED-UNet3+ indicating that it tends to provide better segmentation quality. The distribution of points is limited and symmetrical which highlights the consistency and reliability of its outputs.

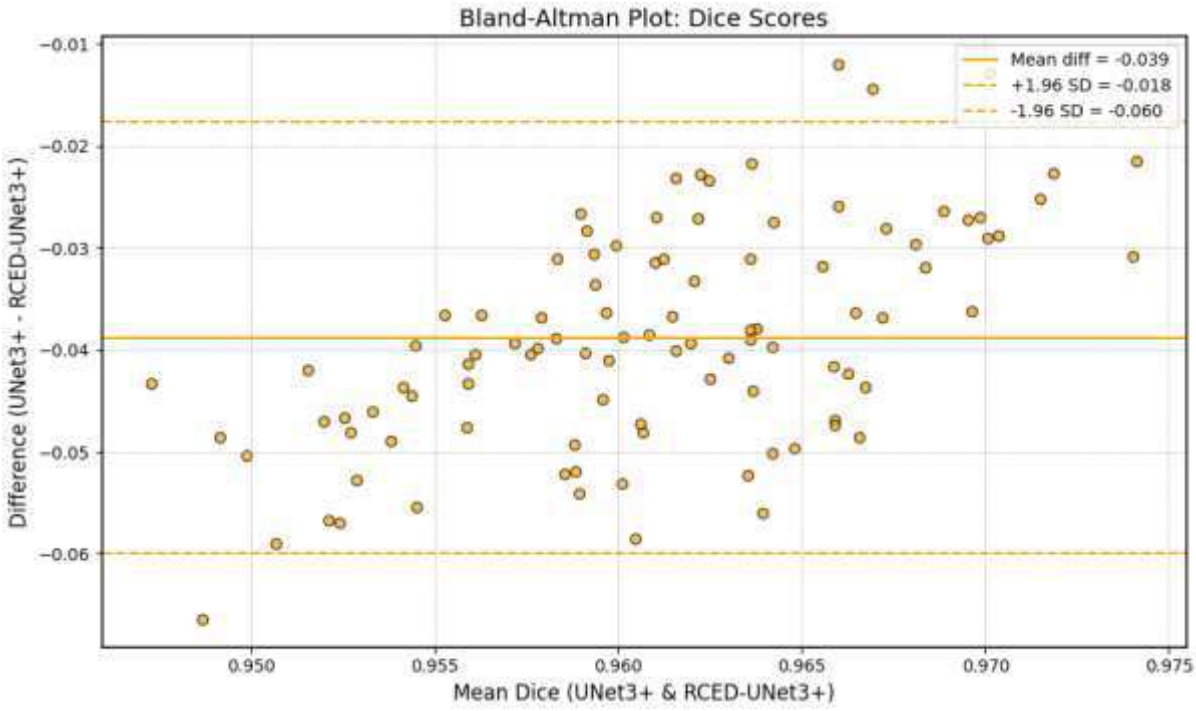

Figure 10: *Dice score differences confirm RCED-UNet3+ performs more consistently and accurately than UNet3+, with minimal variation across test cases.*

The original UNet3+ had the least promising results among the evaluated configurations. RCED-UNet3+ with residual connections enhanced the capability of the model to learn features that are difficult to capture. Increasing the data also enhanced its capability to deal with diverse inputs. In general, both statistical results and qualitative assessment indicate that RCED-UNet3+ provides more precise and consistent segmentation as applied to a large variety of CT images.

5. CONCLUSION

RCED-UNet3+ is a segmentation architecture that integrates residual connections to enhance feature learning and enable the construction of deeper networks. This design overcomes issues of traditional architectures which tend to suffer decreasing performance with increasing network depth hence offering more valid segmentation results. The model utilizes a hybrid loss that is based on Dice loss and binary cross-entropy to have the accuracy of precision on the pixel-level classification and the accuracy of the overlap. The dataset used in training was the LIDC-IDRI dataset whereas the evaluation was done on the LUNA16 and the LIDC-IDRI datasets to gauge the performance of the model with varying data sources. The experiments have shown that RCED-UNet3 + consistently was better than the baseline UNet3 +, which indicates its strength in dealing with the variation in the CT scans. Future enhancements could involve the integration of attention mechanisms and validation using larger, multi-institutional datasets to further improve its adaptability and clinical reliability.

REFERENCE

Soriano, J.B., et al., Prevalence and attributable health burden of chronic respiratory diseases, 1990–2017: a systematic analysis for the Global Burden of Disease Study 2017. *The Lancet Respiratory Medicine,* 2020. **8**(6): p. 585-596.

Siegel, R.L., et al., *Cancer statistics, 2025.* Ca, 2025. **75**(1): p. 10.

Firmino, M., et al., Computer-aided detection (CADe) and diagnosis (CADx) system for lung cancer with likelihood of malignancy. *Biomedical engineering online,* 2016. **15**: p. 1-17.

Zemouri, R., N. Zerhouni, and D. Racoceanu, Deep learning in the biomedical applications: Recent and future status. *Applied Sciences,* 2019. **9**(8): p. 1526.

Mansoor, A., et al., Segmentation and image analysis of abnormal lungs at CT: current approaches, challenges, and future trends. *Radiographics,* 2015. **35**(4): p. 1056-1076.

Hofmanninger, J., et al., Automatic lung segmentation in routine imaging is primarily a data diversity problem, not a methodology problem. *European radiology experimental,* 2020. **4**: p. 1-13.

Chaturvedi, P., et al. Prediction and classification of lung cancer using machine learning techniques. in IOP conference series: *materials science and engineering*. 2021. IOP Publishing.

S. Diciotti, G. Picozzi, M. Falchini, M. Mascalchi, N. Villari *et al.,* "3-D segmentation algorithm of small lung nodules in spiral CT images," *IEEE transactions on Information Technology in Biomedicine,* vol. 12, no. 1, pp. 7-19, 2008.

T. Messay, R. Hardie and S. K. Rogers, "A new computationally efficient CAD system for pulmonary nodule detection in CT imagery," *Medical image analysis,* vol. 14, no. 3, pp. 390-406, 2010.

Y. Yuan and C. He, "Adaptive active contours without edges," *Mathematical and Computer Modelling,* vol. 55, no. 5-6, pp. 1705-1721, 2012.

Y. Boykov and V. Kolmogorov, "An experimental comparison of min-cut/max-flow algorithms for energy minimization in vision," *IEEE transactions on pattern analysis and machine intelligence,* vol. 26, no. 9, pp. 1124-1137, 2004.

J. Dehmeshki, H. Amin, M. Valdivieso and X. Ye, "Segmentation of pulmonary nodules in thoracic CT scans: a region growing approach," *IEEE Transactions on medical imaging,* vol. 27, no. 4, pp. 467-480, 2008.

W. J. Kostis, A. P. Reeves, D. F. Yankelevitz and C. I. Henschke, "Three-dimensional segmentation and growth-rate estimation of small pulmonary nodules in helical CT images," *IEEE Transactions on Medical Imaging*, vol. 22, no. 10, pp. 1259-1274, 2003.

A. O. de C. Filho, W. B. de Sampaio, A. C. Silva, A. C. de Paiva, R. A. Nunes *et al.*, "Automatic detection of solitary lung nodules using quality threshold clustering, genetic algorithm and diversity index," *Artificial intelligence in medicine*, vol. 60, no. 3, pp. 165-177, 2014.

C. Jacobs, E. M. van Rikxoort, T. Twellmann, E. Th. Scholten, P. A. de Jong *et al.*, "Automatic detection of subsolid pulmonary nodules in thoracic computed tomography images," *Medical image analysis*, vol. 18, no. 2, pp. 374-384, 2014.

Ait Skourt, B., A. El Hassani, and A. Majda, Lung CT image segmentation using deep neural networks. *Procedia computer science*, 2018. **127**: p. 109-113.

Shaziya, H., K. Shyamala, and R. Zaheer. Automatic lung segmentation on thoracic CT scans using U-net convolutional network.*International conference on communication and signal processing (ICCSP)*. 2018. IEEE.

Yoo, S.-J., et al., Automated lung segmentation on chest computed tomography images with extensive lung parenchymal abnormalities using a deep neural network. *Korean journal of radiology, 2020.* **22**(3): p. 476.

Raza, S., et al., RCED-UNet3+: Unleashing Residual Connections in Encoder-Decoder Architecture for Precise Lung Nodule Segmentation. *Traitement du Signal, 2024.* **41**(6): p. 3063.

Aversano, L., et al. An enhanced UNet variant for effective lung cancer detection. *International Joint Conference on Neural Networks (IJCNN)*. 2022. IEEE.